Article:

Xie, F, Xia, Y, Feng, W orcid.org/0000-0002-9907-9120 et al. (1 more author) (2023) Increasing Surface UV Radiation in the Tropics and Northern Mid-Latitudes due to Ozone Depletion after 2010. Advances in Atmospheric Sciences, 40. pp. 1833-1843. ISSN 0256-1530

https://doi.org/10.1007/s00376-023-2354-9

Increasing Surface UV Radiation in the Tropics and Northern mid-latitudes due to Ozone Depletion after 2010

Fei XIE[1], Yan XIA[1*], Wuhu FENG[2,3] and Yingli NIU[1]

[1] *School of Systems Science and College of Global Change and Earth System Science, Beijing Normal University, Beijing, China*

[2]*Istitute for Climate and Atmospheric Science, School of Earth and Environment, University of Leeds, Leeds, UK.*

[3]*National Centre for Atmospheric Science, University of Leeds, Leeds, UK.*

Submitted to: ***Advances in Atmospheric Sciences***

* Corresponding author: Dr. Yan Xia (xiayan@bnu.edu.cn)

Abstract

Excessive ultraviolet (UV) exposure harms human and ecosystems. The level of surface UV radiation increased as a result of stratospheric ozone decreases from late 1970s in relation to emissions of chlorofluorocarbons. Following implementation of the Montreal Protocol, the stratospheric loading of chlorine/bromine peaked in the late 1990s and then decreased; so, accordingly, stratospheric ozone and surface UV radiation would be expected to recover and decrease, respectively. Based on multiple data sources, we show here that the May–September surface UV radiation in the tropics and Northern Hemisphere mid-latitudes has a statistically significant increasing trend (about 60.0 J/m^2/decade) at the 2σ level for the period 2010–2020, due to the onset of total column ozone (TCO) depletion (about −3.5 DU/decade). Further analysis shows that the decreasing trend of stratospheric ozone after 2010 could be related to increased stratospheric nitrogen oxides due to increasing emissions of the source gas nitrous oxide (N_2O).

Keywords: Surface UV radiation; Stratospheric ozone; Stratospheric chemistry; N_2O

Article Highlights:

- May–September surface UV radiation in the tropics and NH mid-latitudes shows an increasing trend from 2010 to 2020.
- The significant decreasing trends of lower- and mid-stratospheric ozone jointly contributed to the surface UV radiation increasing.
- The increase in N_2O emissions after 2009 and weakened mid-stratospheric circulation resulting in the stratospheric ozone decrease.

1. Introduction

It is well known that solar ultraviolet (UV) radiation is a major factor in the occurrence of skin cancer and damage to the immune system and DNA in humans (Lucas et al., 2019), and has pronounced impacts on agricultural productivity, terrestrial and aquatic ecosystems, and air quality (Douglass et al., 2011; Williamson et al., 2014). The importance of UV radiation to influence global ecosystems has been widely discussed. Stratospheric ozone is a key factor in modulating the changes of UV radiation at the Earth's surface. Stratospheric ozone levels began declining from the late 1970s (Farman et al., 1985), which was mainly related to human use of chlorine and bromine containing compounds such as chlorofluorocarbons (CFCs) (Molina and Rowland, 1974; Solomon et al., 1986). This decrease in stratospheric ozone led to an increase in surface UV radiation via the creation of a hole in the ozone layer over the Antarctic (Gurney, 1998; Hegglin and Shepherd, 2009; Tourpali et al., 2009; Bais et al., 2015; Eleftheratos et al., 2020). After the Antarctic ozone hole was detected in the 1980s (Farman et al., 1985; Solomon, 1999), the signing of the Montreal Protocol (MP) in 1987 has successfully reduced emissions of ozone-depleting substances. Following the MP, the stratospheric loading of chlorine/bromine peaked in the late 1990s and has since decreased, meaning the level of stratospheric ozone is projected to recover and the related increase in UV radiation at Earth's surface should be abated.

Many studies, however, have reported that whilst upper-stratospheric ozone started recovering from 1995 to 2016 following the MP, ozone in the lower stratosphere is still showing a continual declining trend (Kyrölä et al., 2013; Sofieva et al., 2017; Steinbrecht et al., 2017; Ball et al., 2018, 2019; Bourassa et al., 2018; Petropavlovskikh et al., 2019; Orbe et al., 2020; Dietmüller et al., 2021; Bognar et al., 2022), most likely because of the continued production and release of one particular type of CFC, trichlorofluoromethane (Montzka et al., 2018), or the dynamic transport caused by natural variability (Chipperfield et al., 2018; Dhomse et al., 2018; Morgenstern et al., 2018; Wargan et al., 2018). The LOTUS report (SPARC/IO3C/GAW, 2019) further pointed out that, between January 2000 and December 2016, statistically significant positive ozone trends were obtained throughout the upper stratosphere on the basis of satellite and ground-based data; whereas, though non-significant, negative ozone trends were consistently detected by multiple satellite sources in the post-2000 period for the middle and lower stratosphere over the tropics and Northern Hemisphere (NH) mid-latitudes. Due to this inconsistency between the changes in ozone in the upper and lower stratosphere after the 1990s, the recovery of total ozone column (TCO) is not significant. In addition, there are other challenges to the ozone recovery (Chipperfield, 2009; Daniel et al., 2010; Ravishankara et al., 2009; Wang et al., 2014; Xie et al., 2014; Tian et al., 2017; Lu et al., 2019; Zhang et al., 2019; Hu et al., 2022; Solomon et al., 2022). Here, we find that the TCO in the tropics and Northern Hemisphere mid-latitudes started to significantly deplete again in the May-September period after around 2010, resulting in increasing surface UV radiation.

2. Methods

2.1 Observations

The UV data (including cloud effects) in this study are from the Ozone Monitoring Instrument (OMI) and Tropospheric Emission Monitoring Internet Service (TEMIS) datasets; the ozone data are from the Multi-Sensor Reanalysis 2 (MSR-2), the The Stratospheric Water and OzOne Satellite Homogenized (SWOOSH) and Microwave Limb Sounder (MLS) datasets; and the ClO, BrO and HNO_3 data are from the MLS dataset. The OMI dataset (Hovila et al., 2013) with horizontal resolution of 1° × 1° is used. In the TEMIS dataset (Van Geffen et al., 2017), the UV index and UV dose data of version 2.2 are given on a latitude–longitude grid of 0.25° × 0.25° covering the whole globe. For MSR-2 (Van Der et al., 2015), the monthly mean total column ozone spans the period 1979–2020 with a horizontal resolution of 0.5° × 0.5°. The SWOOSH dataset (Davis et al., 2016) with a 2.5° zonal mean value is used. The MLS (Livesey et al., 2015), version 5, measures daily atmospheric chemical species with a global coverage from 82°N to 82° S and a vertical resolution of ~3 km.

2.2 Model and simulation

The TOMCAT/SLIMCAT three-dimensional offline chemical transport model (Chipperfield, 2006; Feng et al., 2021) is used to investigate the processes of ozone-related chemistry. The model uses horizontal temperature and wind from the European Centre for Medium-Range Weather Forecasts (Hersbach et al., 2020) (ERA5). In this study, a historical reproduction experiment was run with horizontal resolution of about 2.8° latitude × 2.8° longitude and 32 levels from the surface to 65 km. The model provides a good representation of stratospheric chemistry compared with observations (Chipperfield, 2006; Feng et al., 2011).

3. Increasing UV radiation changes related to ozone depletion

Figures 1(a)–(c) show the UV changes at surface level from 2005 to 2020 at different latitudes obtained from the Ozone Monitoring Instrument (OMI) and Tropospheric Emission Monitoring Internet Service (TEMIS) data. For a description of the data please refer to Methods section. Due to the sparse population at the poles, we focus only on the UV changes between 60°S and 60°N. We find that surface UV shows increasing trends over the tropics and NH mid-latitudes (Figures 1b and c) but a decreasing trend over Southern Hemisphere (SH) mid-latitudes (Figure 1a) from around

2010 onwards. The linear trends are −34.2 ± 14.7 J/m^2/decade, 54.4 ± 14.3 J/m^2/decade and 78.0 ± 17.3 J/m^2/decade over the SH mid-latitudes (Figure 1a), tropics (Figure 1b) and NH mid-latitudes (Figure 1c), respectively, for the period 2010–2020 (significant at the 2σ level using the Student's *t*-test). The results from the two datasets show a high degree of consistency.

TCO is one of the main drivers of changes in surface UV. Figures 1(d)–(f) show the changes in TCO from 2005 to 2020 at different latitudes between 60°S and 60°N obtained from the Multi-Sensor Reanalysis 2 (MSR-2) and The Stratospheric Water and OzOne Satellite Homogenized (SWOOSH) data (see Methods). From around 2010 onward, the UV trends are in close agreement with those of TCO. That is, the linear trends of ozone are 4.2 ± 1.1 DU/decade (Figure 1d), −1.7 ± 0.5 DU/decade (Figure 1e) and −5.5 ± 1.9 DU/decade (Figure 1f) in the SH mid-latitudes, tropics and NH mid-latitudes, respectively, for the period 2010–2020 (significant at the 2σ level using the Student's *t*-test). The correlation coefficients over this period between TCO and UV variations are −0.51, −0.95 and −0.88 in the SH mid-latitudes, tropics and NH mid-latitudes, respectively, which demonstrates that the changes in TCO played a key role in the changes of UV during this period. It should be noted that, aside from ozone, factors such as cloud cover, aerosols, air pollutants and surface reflectance also affect UV (Kylling et al., 2000; Bernhard et al., 2007; den Outer et al., 2010; Douglass et al., 2011). The positive trend of TCO in the SH mid-latitudes (Weber et al., 2022) (Figure 1d) may be related to decreasing emissions of ozone depletion substances, resulting in the negative trend of UV (Figure 1a). Next, we would focus on investigating the significant decreasing TCO trends over the tropics and NH mid-latitudes (Figures 1e and f), which are responsible for the increasing UV trends (Figures 1b and c).

Figure 2 presents the TCO changes in the tropics and NH mid-latitudes for each month from 2010 to 2020. The linear decreasing TCO trends are strong and significant mainly during May–September. Figure 3 shows the UV and TCO changes in the 30°S–60°N latitudinal belt from 2010 to 2020 averaged from May to September and October to April. The positive UV trend for the May–September average is statistically significant at the 2σ level (Figure 3a), and much larger than that for the October– April average (Figure 3b). This is because the ozone depletion over 30°S–60°N for the May–September average is strong and statistically significant at the 2σ level (Figure 3c), but it is much weaker for the October– April average (Figure 3d). Note that the correlation coefficient between TCO and UV variations for the May–September average is −0.94, which further supports that the changes in TCO leaded to the changes of surface UV during this period.

To further understand the TCO changes in Figures 1 and 3, Figures 4(a)–(d) show the partial column ozone anomalies integrated between different pressure levels of the stratosphere and averaged over 30°S–60°N from 2010 to 2020 based on SWOOSH data. SWOOSH ozone data contain the vertical profile of observed ozone, and the above analysis also shows that its TCO changes are highly consistent with other observational data. From 2010 to 2020, the upper stratospheric ozone still shows a significantly positive trend (Figure 4b), as seen from 2000 to 2016 (Kyrölä et al., 2013; Ball et al., 2018, 2019; SPARC/IO3C/GAW, 2019); In contrast, the mid- and lower-stratospheric ozone shows decreasing but non-significant trends from 2000 to 2016 (Kyrölä et al., 2013; Ball et al., 2018, 2019; SPARC/IO3C/GAW, 2019), but from 2010 to 2020 the decreasing trends are strong and significant at the 2σ level (Figures 4c and d). Figures 4(b)–(d) demonstrate that the significant decreasing trends of lower- and mid-stratospheric ozone jointly contributed to the ozone depletion of the whole stratosphere (Figure 4a), and TCO depletion (Figures 1e and f), from 2010 to 2020.

The partial column ozone anomalies integrated between different pressure levels of the stratosphere and averaged over 30°S–60°N from 2010 to 2020 for May–September and for October–April are also shown in Figures 4(e)–(l). We find that upper/lower stratospheric ozone is increasing/decreasing for both May–September (Figures 4f and h) and October–April (Figures 4j and l); while the decreasing trend of mid-stratospheric ozone is significant and strong for May–September (Figure 4g) but non-significant and weak for October–April (Figure 4k). Since the middle stratosphere is the layer with the largest ozone concentration, the partial column ozone trend for the whole stratosphere is much weaker in October–April compared to that in May–September (Figure 4e vs 4i). Figures 4(e)–(l) imply that the decrease in mid-stratospheric ozone for May–September may be the main reason for the decreasing trends of TCO and increasing trends of surface UV being significant and strong from 2010 to 2020 during May–September (Figure 3) but not during other months.

Figure 5 shows the TCO changes averaged at different latitudes between 60°S to 60°N from 2005 to 2020 for the May–September average based on the TOMCAT/SLIMCAT simulation (see Methods section). The results show that the model simulates the recent decreasing trends of TCO since 2010 over the tropics and NH mid-latitudes (Figures 5b and Sc) and increasing trend over SH mid-latitudes (Figure 5a); however, the decreasing trends are weaker and non-significant compared with the observations (Figures 5b, c vs Figures 1e, f). Figure 6 shows the partial column ozone integrated between different altitudes and averaged over 30°S–60°N from 2005 to 2020 for the May–September based on the TOMCAT/SLIMCAT simulation. Consistent with observations (Figures 4f and g), the model simulates a positive trend of upper-stratospheric ozone and negative trend of mid-stratospheric ozone (Figures 6b and c). However, the strongly negative trend of lower-stratospheric ozone in the observed data (Figures 4d, h and l) is not reproduced by the model (Figure 6d). Thus, the simulated ozone trend in the whole stratosphere is smaller (–0.8 DU/decade, Figure 6a), resulting in the simulated decreasing TCO trends over the tropics and NH mid-latitudes are weaker and less significant compared with the observations (Figures 5b, c vs Figures 1e, f).

4. Influence of increased stratospheric nitrogen oxides on ozone depletion

In general, the TOMCAT/SLIMCAT model simulates the recent trends of ozone since around 2010 reasonably well, so the mechanisms responsible for the ozone depletion during 2010–2020 are further investigated using both observations and the simulation results. Figure 7 shows the fractional trends of zonal-mean ozone and the related chemical components from 2010 to 2020 for May–September. We find that ozone exhibits a decreasing trend in most regions of the mid-lower stratosphere (below 10 hPa) in the tropics and NH mid-latitudes. This feature is highly consistent among the SWOOSH data, Microwave Limb Sounder (MLS) data and the TOMCAT/SLIMCAT simulation (Figures 7a–c). However, the ozone depletion in the mid-lower stratosphere is much weaker in TOMCAT/SLIMCAT than in the SWOOSH and MLS data, and this explains why the simulated decreasing trends of TCO (Figures 5b and c) are much weaker compared to the observations (Figures 1e and f). Figures 7(a)–(c) further corroborate that the significant decrease in the mid- and lower-stratospheric ozone together led to the significantly negative trend in the TCO over the tropics and NH mid-latitudes in the past decade (Figures 1e and f).

Active chlorine ($Cl_x = Cl + ClO + Cl_2O_2$) and bromine ($Br_x = Br + BrO$) are among the most important chemical components for ozone depletion. Figures 7(d)–(g) show the Cl_x and Br_x linear trends from 2010 to 2020 for May–September based on MLS data and the TOMCAT/SLIMCAT simulation. For the upper and middle stratosphere, Cl_x (Cl_2O_2 isn't included) and Br_x are in decline from 2010 to 2020, which would be conducive to upper stratospheric ozone recovery but cannot explain the decreasing mid-stratospheric ozone. For the lower stratosphere, ClO is increasing in MLS data (Figure 7d). The increase in ClO agrees with the strong ozone depletion in the lower stratosphere in the SWOOSH and MLS data (Figures 7a and b). The TOMCAT/SLIMCAT simulation shows different results from MLS (Figures 7d and e). Cl_x decreases significantly in the lower stratosphere in TOMCAT/SLIMCAT (Figure 7e); the ClO in the TOMCAT/SLIMCAT simulation also has the same characteristics (not shown). This explains why the magnitude of the ozone decline in the lower stratosphere is much smaller in TOMCAT/SLIMCAT (Figure 7c) than in the SWOOSH and MLS data (Figures 7a and b), and also implies that Cl_x may be a cause of the lower stratospheric ozone reduction after 2010. The increase in Cl_x in the lower stratosphere may be related to increasing emissions of short-lived chlorine source gases not considered in the model, but these aspects are not further discussed in the present paper.

It is found that stratospheric NO_x increases significantly in the tropics and NH mid-latitudes, especially over 30°S–60°N, from 2010 to 2020 (Figures 7h and i). In Figure 7h we replace the changes in NO_x with observed HNO_3 because HNO_3 is a major reservoir of NO_x in the stratosphere and an increase in HNO_3 can serve as a good representation of any increase in NO_x. NO_x can react to deplete stratospheric ozone (Crutzen, 1970) and is considered to be one of the important factors affecting ozone recovery (Chipperfield, 2009; Ravishankara et al., 2009). Note that the spatial patterns in Figures 7h and i are closely consistent with those in Figures 7(a)–(c) in the middle stratosphere, which implies that the increasing NO_x may be a main reason for the decrease in mid-stratospheric ozone. In summary, according to above analysis, the decrease in mid-stratospheric ozone may be the main reason for the decreasing trend of TCO and increasing trend of surface UV being significant and strong from 2010 to 2020 for May–September, and the increasing NO_x for May–September likely plays a key role in influencing these significant decreasing trend of mid-stratospheric ozone.

One more question of interest is why the mid-stratospheric ozone depletion or, for example, the increase in NO_x, mainly occurred in the tropics and NH mid-latitudes after 2010 for May–September. Nitrous oxide (N_2O) is highly stable in the troposphere until it is transported into the stratosphere, where its chemical decomposition is the primary source of stratospheric NO_x (Chang, 2003). Previous studies have pointed out that the increase of N_2O mainly influence mid-stratospheric ozone (Chipperfield, 2009; Ravishankara et al., 2009). It is important to note that global N_2O emissions accelerated substantially after 2009 (Thompson et al., 2019) (Figure 8), which might be a reason for the significant increase in stratospheric NO_x after 2010. On the other hand, the chemical decomposition of N_2O is also related to the strength of the stratospheric circulation. Weakened meridional transport with older air is characterized by a larger relative conversion of N_2O into NO_x. Figure 9 shows the fractional trends of the age-of-air for May–September and for October–April based on the TOMCAT/SLIMCAT simulation from 2010–2020. Clearly, the trends in the age-of-air for May–September are larger than those for October–April in the middle stratosphere over 30°S–60°N during 2010 to 2020 (Figures 9a–c). The larger/smaller trends of the age-of-air correspond to larger/smaller trends of NO_x (Figures 9d–f) in the middle stratosphere, which helps to explain why the mid-stratospheric ozone depletion mainly occurred during May–September.

5. Conclusions

This study finds that surface UV radiation in the tropics and NH mid-latitudes shows a statistically significant increasing trend at the 2σ level from 2010 to 2020 for the months of May–September due to the beginning of TCO depletion. The significant decreasing trends of lower- and mid-stratospheric ozone jointly contributed to the TCO depletion from 2010 to 2020, and the decrease in mid-stratospheric ozone for May–September may be the main reason for the decreasing trends of TCO being significant and strong from 2010 to 2020 during May–September but not during other months. The increase in N_2O emissions after 2009 and weakened mid-stratospheric circulation for May–September is found to possibly have caused increasing NO_x in the stratosphere, resulting in the mid-stratospheric ozone being significantly depleted after 2010 for May–September. Since N_2O is the primary source of stratospheric NO_x, our results presented here further support those predicted by previous studies (Randeniya et al., 2002; Chipperfield, 2009; Ravishankara et al., 2009), i.e., that N_2O emissions delay ozone recovery. More importantly, this study demonstrates that N_2O emissions not only delay ozone future recovery, but even lead to a depletion in TCO and an increase in surface UV radiation in May–September in the tropics and NH mid-latitudes in the current environment with global warming. This unexpected ozone depletion and UV increase might pose more serious threats (including increased incidence of skin cancers and ecological damage) than that at the poles, since the tropics and NH mid-latitudes are densely populated and economically developed regions.

Data availability statement

Data related to this paper are publicly available and can be downloaded from the following addresses: OMI from https://acdisc.gesdisc.eosdis.nasa.gov/data/Aura_OMI_Level3/OMUVBd.003/;

TEMIS from https://www.temis.nl/uvradiation/UVdose.php; MSR-2 from https://www.temis.nl/protocols/O3global.php; SWOOSH from http://www.esrl.noaa.gov/csd/groups/csd8/swoosh/; MLS from https://mls.jpl.nasa.gov/. TOMCAT/SLIMCAT data are available online at https://doi.org/10.5281/zenodo.6970461. The codes to calculate the results associated with the main figures in this study are available from the corresponding author upon reasonable request.

Acknowledgments

We acknowledge the OMI, TEMIS, MSR-2, SWOOSH and MLS teams for providing the observational data used in this study. Funding for this work was provided by the National Natural Science Foundation of China (42122037, 42105016, 41975047).

REFERENCES

Bais A F, McKenzie R L, Bernhard G, Aucamp P J, Ilyas M, Madronich S and Tourpali K 2015 Ozone depletion and climate change: Impacts on UV radiation *Photochem. Photobiol. Sci.* **14** 19–52.

Ball W T, Alsing J, Mortlock D J, Staehelin J, Haigh J D, Peter T, Tummon F, Stubi R, Stenke A, Anderdon J, Bourassa A, Davis S M, Degenstein D, Frith S, Froidevaux L, Roth C, Sofieva V, Wang R, Wild J, Yu P, Ziemke J R and Rozanov E V 2018 Evidence for a continuous decline in lower stratospheric ozone offsetting ozone layer recovery *Atmos. Chem. Phys*. **18** 1379–1394.

Ball W T, Alsing J, Staehelin1 J, Davis S M, Froidevaux L and Peter T 2019 Stratospheric ozone trends for 1985–2018: sensitivity to recent large variability *Atmos. Chem. Phys*. **19** 12731–12748.

Bernhard G, Booth C R, Ehramjian J C, Stone R and Dutton E G 2007 Ultraviolet and visible radiation at Barrow, Alaska: Climatology and influencing factors on the basis of version 2 National Science Foundation network data *J. Geophys. Res.* **112** D09101.

Bognar K, Tegtmeier S, Bourassa A, Roth C, Warnock T, Zawada D and Degenstein D 2022 Stratospheric ozone trends for 1984–2021 in the SAGE II–OSIRIS–SAGE III/ISS composite dataset *Atmos. Chem. Phys.* **22** 9553–9569.

Bourassa A E, Roth C Z, Zawada D J, Rieger L A, McLinden C A and Degenstein D A 2018 Drift-corrected Odin-OSIRIS ozone product: algorithm and updated stratospheric ozone trends *Atmos. Meas. Tech.* **11** 489–498.

Chang M E 2003 Chemistry of Atmospheres: R.P. Wayne (Ed.), Oxford University Press, Oxford, third ed., 2000, ISBN 0-19-850375-X *Agric. For Meteorol.* **118** 143–144.

Chipperfield M P 2006 New version of the TOMCAT/SLIMCAT off-line chemical transport model: Intercomparison of stratospheric tracer experiments *Q.J.R. Meteorol. Soc*. **132** 1179–1203.

Chipperfield M P 2009 Nitrous oxide delays ozone recovery *Nat. Geosci*. **2** 742–743.

Chipperfield M P, Dhomse S, Hossaini R, Feng W, Santee M L, Weber M, Burrows J P, Wild J D, Loyola D and Egbers M C 2018 On the cause of recent variations in lower stratospheric ozone *Geophys. Res. Lett*. **45** 5718–5726.

Crutzen P J 1970 The influence of nitrogen oxides on the atmospheric ozone content *Q. J. R. Meteorol. Soc*. **96** 320–325.

Daniel J S, Fleming E L, Velders G J M, Jackman C H and Ravishankara A R 2010 Options to accelerate ozone recovery: ozone and climate benefits *Atoms. Chem. Phys*. **10** 7697–7707.

Davis S M, Rosenlof K H, Hassler B, Hurst D F, Read W G, Vömel H, Selkirk H, Fujiwara M and Damadeo R 2016 The Stratospheric Water and Ozone Satellite Homogenized (SWOOSH) database: a long-term database for climate studies *Earth Syst. Sci. Data*. **8** 461–490.

Dhomse S S et al 2018 Estimates of ozone return dates from Chemistry Climate Model Initiative simulations *Atmos. Chem. Phys*. **18** 8409–8438.

den Outer P N, Slaper H, Kaurola J, Lindfors A, Kazantzidis A, Bais A F, Feister U, Junk J, Janouch M and Josefsson W 2010 Reconstructing of erythemal ultraviolet radiation levels in Europe for the past 4 decades *J. Geophys. Res*. **115** D10102.

Dietmüller S, Garny H, Eichinger R and Ball W T 2021 Analysis of recent lower-stratospheric ozone trends in chemistry climate models *Atmos. Chem. Phys*. **21** 6811–6837.

Douglass A et al 2011 Stratospheric ozone and surface ultraviolet radiation. In Scientific assessment of ozone depletion: 2010, Global Ozone Research and Monitoring Project (Report No. 52, Chapter 2). Geneva, Switzerland: World Meteorological Organization..

Eleftheratos K K, Zerefos J, Bais C S, Fountoulakis A F, Dameris I, Joeckel M, Haslerud P, Godin-Beekmann A S, Steinbrecht S, Petropavlovskikh W, Brogniez I, Leblanc C, Liley T, Ben Querel J, Swart R and Daan P J 2020 Possible Effects of Greenhouse Gases to Ozone Profiles and DNA Active UV-B Irradiance at Ground Level *Atmosphere* **11** 228.

Farman J C, Gardiner B G and Shanklin J D 1985 Large losses of total ozone in Antarctica reveal seasonal ClOx/NOx interaction *Nature* **315** 207–210.

Feng W, Chipperfield M P, Davies S, Mann G W, Carslaw K S, Dhomse S, Harvey L, Randall C and Santee M L 2011 Modelling the effect of denitrification on polar ozone depletion for Arctic winter 2004/2005 *Atmos. Chem. Phys*. **11** 6559–6573.

Feng W, Dhomse S, Arosio C, Weber M, Burrows J P, Santee M L and Chipperfield M P 2021 Arctic ozone depletion in 2019/20: Roles of chemistry, dynamics and the Montreal Protocol *Geophys. Res. Lett*. **48.**

Gurney K R 1998 Evidence for increasing ultraviolet irradiance at Point Barrow Alaska *Geophys. Res. Lett.* **25** 903–906.

Hegglin M I and Shepherd T G 2009 Large climate-induced changes in ultraviolet index and stratosphere-to-troposphere ozone flux *Nat. Geosci*. **2** 687–691.

Hersbach H et al 2020 The ERA5 global reanalysis *Q.J.R. Meteorol. Soc.* **146** 1999–2049.

Hovila J, Arola A and Tamminen J 2013 OMI/Aura Surface UVB Irradiance and Erythemal Dose Daily L3 Global Gridded 1.0 degree x 1.0 degree V3. NASA Goddard Space Flight Center, Goddard Earth Sciences Data and Information Services Center (GES DISC).

Hu D Guan Z Liu M and Feng W 2022 Dynamical mechanisms for the recent ozone depletion in the Arctic stratosphere linked to the North Pacific sea surface temperatures *Climate Dynamics*, **58**(20), https://doi.org/10.1007/s00382-021-06026-x

Kylling A, Dahlback A and Mayer B 2000 The effect of clouds and surface albedo on UV irradiances at a high latitude site *Geophys. Res. Lett.*, **27** 1411–1414.

Kyrölä E, Laine M, Sofieva V, Tamminen J, Päivärinta S M, Tukiainen S and Thomason L 2013 Combined SAGE II–GOMOS ozone profile data set for 1984–2011 and trend analysis of the vertical distribution of ozone *Atmos. Chem. Phys.* **13** 10645–10658.

Livesey N J et al 2015 EOS MLS Version 4.2x Level 2 data quality and description document *New York, NY: Rev., B. Jet Propulsion Laboratory*, **D-33509.**

Lu J, Xie F, Tian W, Li J, Feng W, Chipperfield M, Zhang J, and Ma X 2019 Interannual variations in lower stratospheric ozone during the period 1984–2016 *J. Geophys. Res.* **124** 8225–8241.

Lucas R M, Yazar S, Young A R, Norval M, de Gruijl F R, Takizawa Y, Rhodes L E, Sinclair C A and Neale R E 2019 Human health in relation to exposure to solar ultraviolet radiation under changing stratospheric ozone and climate *Photochem. Photobiol. Sci*. **18** 641.

Molina M J and Rowland F S 1974 Stratospheric sink for chlorofluoromethanes: chlorine atom-catalysed destruction of ozone *Nature* **249** 810–812.

Montzka S A, Dutton G S, Yu P, Ray E, Portmann R W, Daniel J S, Kuijpers L, Hall B D, Mondeel D, Siso C, Nance J D, Rigby M, Manning A J, Hu L, Moore F, Miller B R and Elkins J W 2018 An unexpected and persistent increase in global emissions of ozone-depleting CFC-11 *Nature* **557** 413–417.

Morgenstern O, Stone K A, Schofield R, Akiyoshi H, Yamashita Y, Kinnison D E, Garcia R R, Sudo K, Plummer D A, Scinocca J, Oman L D, Manyin M E, Zeng G, Rozanov E, Stenke A, Revell L E, Pitari G, Mancini E, Di Genova G, Visioni D, Dhomse S S and Chipperfield M P 2018 Ozone sensitivity to varying greenhouse gases and ozone-depleting substances in CCMI-1 simulations *Atmos. Chem. Phys.* **18** 1091–1114.

Orbe C, Wargan K, Pawson S and Oman L D 2020 Mechanisms linked to recent ozone decreases in the Northern Hemisphere lower stratosphere *J. Geophys. Res*. **125** e2019JD031631.

Petropavlovskikh I, Godin-Beekmann S, Hubert D, Damadeo R, Hassler B and Sofieva V 2019 SPARC/IO3C/GAW Report on Long-term Ozone Trends and

Uncertainties in the Stratosphere SPARC Report No. 9; GAW Report No. 241; WCRP Report 17/2018, https://doi.org/10.17874/f899e57a20b, 2019 (code available at: https://arg.usask.ca/docs/LOTUS_regression/index.html, last access: 15 March 2022).

Prather M J 1986 Numerical advection by conservation of second-order moments *J. Geophys. Res*. **91** 6671–6681.

Randeniya L K, Vohralik P F and Plumb I C 2002 Stratospheric ozone depletion at northern mid latitudes in the 21st century: The importance of future concentrations of greenhouse gases nitrous oxide and methane *Geophys. Res. Lett.* **29** 4.

Ravishankara A R, Daniel J S and Portmann R W 2009 Nitrous Oxide (N2O): The Dominant Ozone-Depleting Substance Emitted in the 21st Century *Science*. **326** 123–125.

Sofieva V F, Kyrölä E, Laine M, Tamminen J, Degenstein D, Bourassa A, Roth C, Zawada D, Weber M, Rozanov A, Rahpoe N, Stiller G, Laeng A, von Clarmann T, Walker K A, Sheese P, Hubert D, van Roozendael M, Zehner C, Damadeo R, Zawodny J, Kramarova N and Bhartia P K 2017 Merged SAGE II, Ozone_cci and OMPS ozone profile dataset and evaluation of ozone trends in the stratosphere *Atmos. Chem. Phys.* **17** 12533–12552.

Solomon S, Garcia R R, Rowland F S and Wuebbles D J 1986 On the depletion of Antarctic ozone *Nature* **321** 755–758.

Solomon S 1999 Stratospheric ozone depletion: A review of concepts and history *Rev. Geophys.* **37** 275–316.

Solomon S, Dube K, Stone K, Yu P, Kinnison D, Toon O B, Strahan S E, Rosenlof K H, Portmanng R, Davis S, Randel W, Bernath P, Boone C, Bardeen C G, Bourassab A, Zawada D and Degenstein D 2022 On the stratospheric chemistry of midlatitude wildfire smoke *Proc. Natl. Acad. Sci. USA*. **119** e2117325119.

SPARC/IO3C/GAW, 2019: SPARC/IO3C/GAW Report on Long-term Ozone Trends and Uncertainties in the Stratosphere. I. Petropavlovskikh, S. Godin-Beekmann, D. Hubert, R. Damadeo, B. Hassler, V. Sofieva (Eds.), SPARC Report No. 9, GAW Report No. 241, WCRP-17/2018, doi: 10.17874/f899e57a20b, available at www.sparc-climate.org/publications/sparc-reports.

Steinbrecht W et al 2017 An update on ozone profile trends for the period 2000 to 2016 *Atmos. Chem. Phys.* **17** 10675–10690.

Thompson R L, Lassaletta L, Patra P K, Wilson C, Wells K C, Gressent A, Koffi E N, Chipperfield M P, Winiwarter W, Davidson E A, Tian H and Canadell J G 2019 Acceleration of global N2O emissions seen from two decades of atmospheric inversion *Nat. Clim. Change* **9** 993–998.

Tian W, Li Y, Xie F, Zhang J, Chipperfield M P, Feng W, Hu Y, Zhao S, Zhou X, Yang Y and Ma X 2017 The relationship between lower-stratospheric ozone at southern high latitudes and sea surface temperature in the East Asian marginal seas in austral spring *Atmos. Chem. Phys.* **17** 6705–6722.

Tourpali K, Bais A F, Kazantzidis A, Zerefos C S, Akiyoshi H, Austin J, Brühl C, Butchart N, Chipperfield M P, Dameris M, Deushi M, Eyring V, Giorgetta M A, Kinnison D E, Mancini E, Marsh D R, Nagashima T, Pitari G, Plummer D A, Rozanov E, Shibata K and Tian W 2009 Clear sky UV simulations for the 21st century based on ozone and temperature projections from Chemistry-Climate Models *Atmos. Chem. Phys*. **9** 1165–1172.

Van Der A R, Allaart M A F and Eskes H J 2015 Extended and refined multi sensor reanalysis of total ozone for the period 1970–2012 *Atmos. Meas. Tech*. **8** 3021–3035.

Van Geffen J, Van Weele M, Allaart M and Van Der A R 2017 TEMIS UV index and UV dose operational data products, version 2. Dataset. Royal Netherlands Meteorological Institute (KNMI).

Wang W, Tian W, Dhomse S, Xie F, Shu J and Austin J 2014 Stratospheric ozone depletion from future nitrous oxide increases *Atmos. Chem. Phys*. **14** 12967–12982.

Wargan K, Orbe C, Pawson S, Ziemke J R, Oman L D, Olsen M A, Coy L and Knowland K E 2018 Recent decline in extratropical lower stratospheric ozone attributed to circulation changes *Geophys. Res. Lett*. **45** 5166–5176.

Weber M, Arosio C, Coldewey-Egbers M, Fioletov V E, Frith S M, Wild J D, Tourpali K, Burrows J P and Loyola D 2022 Global total ozone recovery trends attributed to ozone-depleting substance (ODS) changes derived from five merged ozone datasets *Atmos. Chem. Phys*. **22** 6843–6859.

Williamson C E, Richard G Z, Robyn M L, Madronich S, Austin A T, Ballaré C L, Norval M, Sulzberger B, Bais A F, McKenzie R L, Robinson S A, Häder Donat-P, Paul N D and Bornman J F 2014 Solar ultraviolet radiation in a changing climate *Nat. Clim. Change.* **4** 434–441.

Xie F, Li J, Tian W and zhang J 2014 The Relative Impacts of El Niño Modoki, Canonical El Niño, and QBO on Tropical Ozone Changes since the 1980s *Environ. Res. Lett.* 9 064020.

Zhang, J., et al., 2018: Stratospheric ozone loss over the Eurasian continent induced by the polar vortex shift *Nat. Commun.* **9** 206.

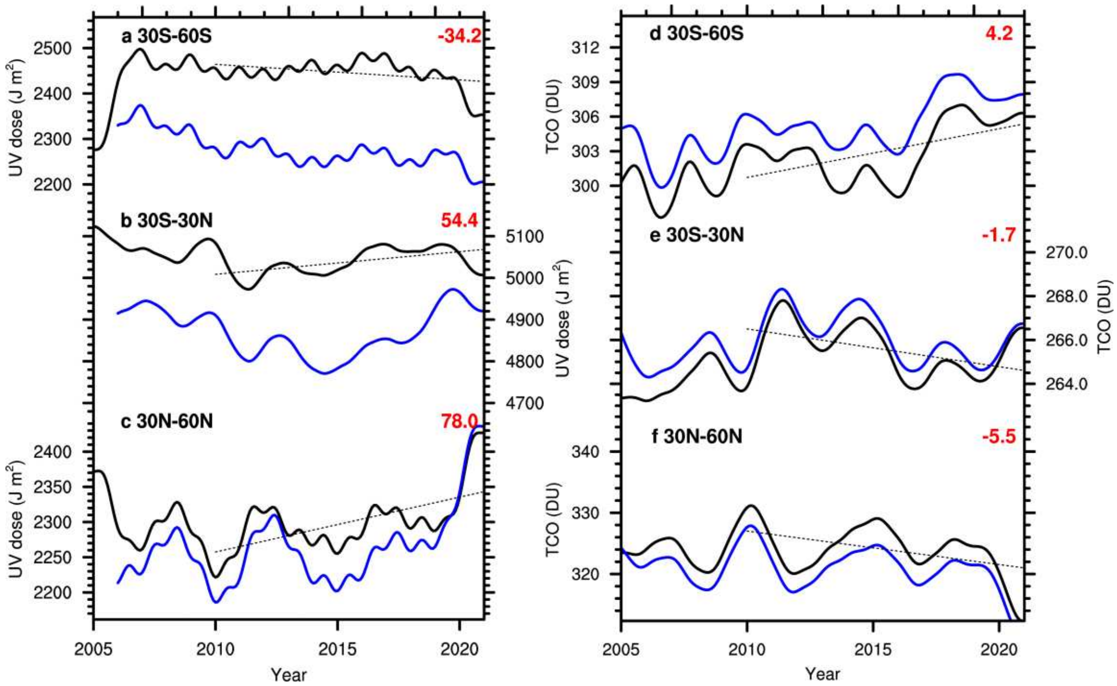

Fig. 1. The UV and TCO changes between different latitudinal belts from 2005 to 2020. The UV (a–c) and TCO (d–f) changes between 60°S and 30°S (a, d), between 30°S and 30°N (b, e), and between 30°N and 60°N (c, f). UV is based on OMI (black line) and TEMIS (blue line) data; TCO is based on MSR-2 (black line) and SWOOSH (blue line) data. For data information, please refer to the Methods section. Linear trends (black straight dotted lines) are calculated by linear regression. The number close to the right-hand *y*-axis is the linear trend value for the period 2010–2020 based on the OMI dataset for UV and based on the MSR-2 dataset for TCO. The red and black values are significant and non-significant, respectively, at the 2σ level using the Student's *t*-test. The unit for the UV trend is J/m^2/decade, and for the TCO trend it is DU/decade. Low-pass filtering (to filter out periods less than 3 years) was performed on the UV and TCO changes before calculating the trend.

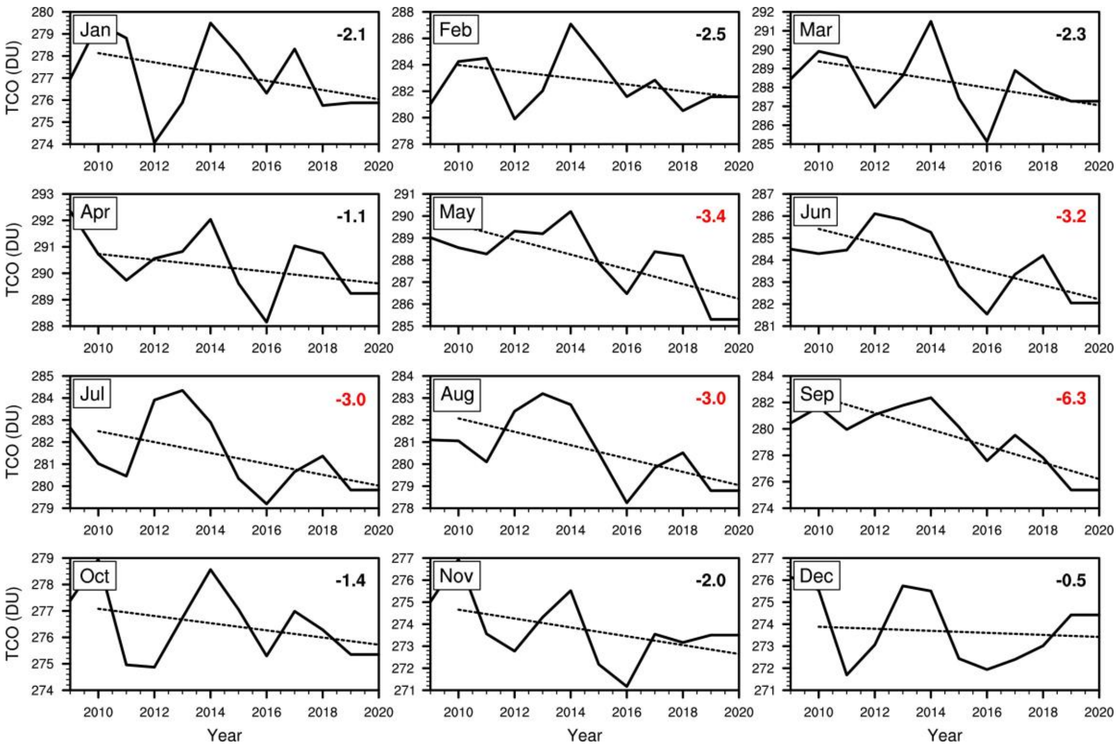

Figure 2. TCO trends in the 30°S–60°N latitudinal belt from 2010 to 2020 for 12 months. The TCO is based on the MSR-2 dataset. For data information, please refer to the Methods section. The linear trends (black straight dotted lines) were calculated by linear regression. The number close to the right-hand *y*-axis is the linear trend value (unit: J/m^2/decade) for the period 2010–2020. Red and black values are significant and non-significant, respectively, at the 2σ level using the Student's *t*-test. A three-point running average was performed on the TCO changes for 12 months before calculating the trend.

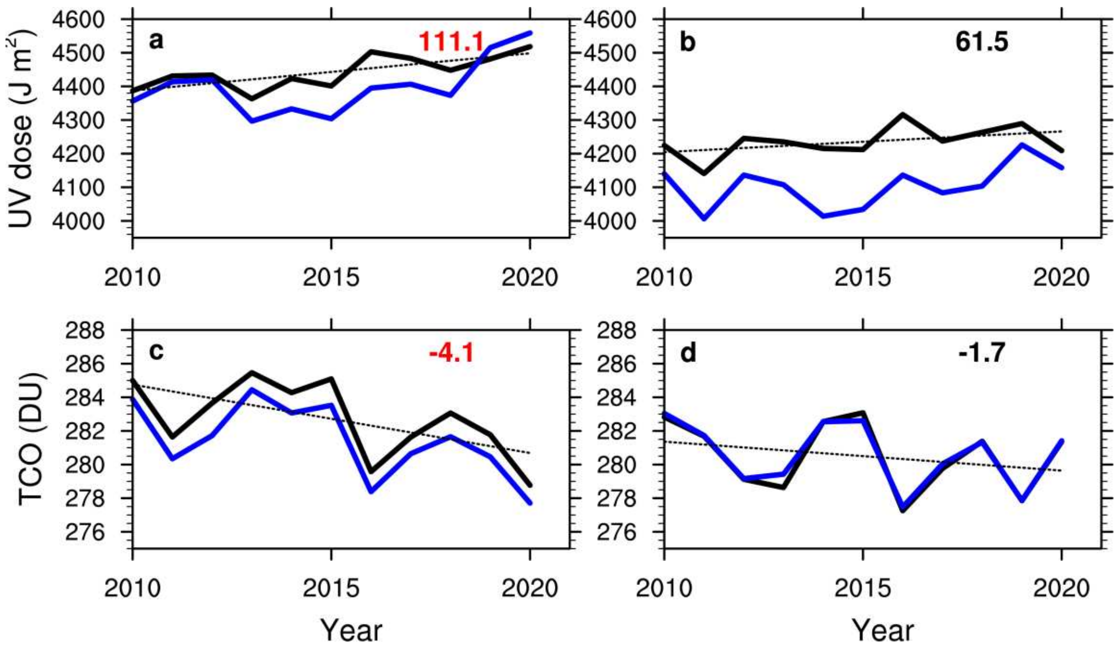

Fig. 3. The UV and TCO changes in the 30°S–60°N latitudinal belt from 2010 to 2020 for the May–September average and the October–April average. The UV (a, b) and TCO (c, d) for the May–September average (a, c) and the October–April average (b, d). UV is based on OMI (black line) and TEMIS (blue line) data; TCO is based on MSR-2 (black line) and SWOOSH (blue line) data. For data information, please refer to the Methods section. Linear trends (black straight dotted lines) are calculated by linear regression. The number close to the right-hand *y*-axis is the linear trend value for the period 2010–2020 based on the OMI dataset for UV and based on the MSR-2 dataset for TCO. Red and black values are significant and non-significant, respectively, at the 2σ level using the Student's *t*-test. The unit for the UV trend is J/m^2/decade, and for the TCO trend it is DU/decade. A three-point running average was performed on the UV and TCO changes before calculating the trend.

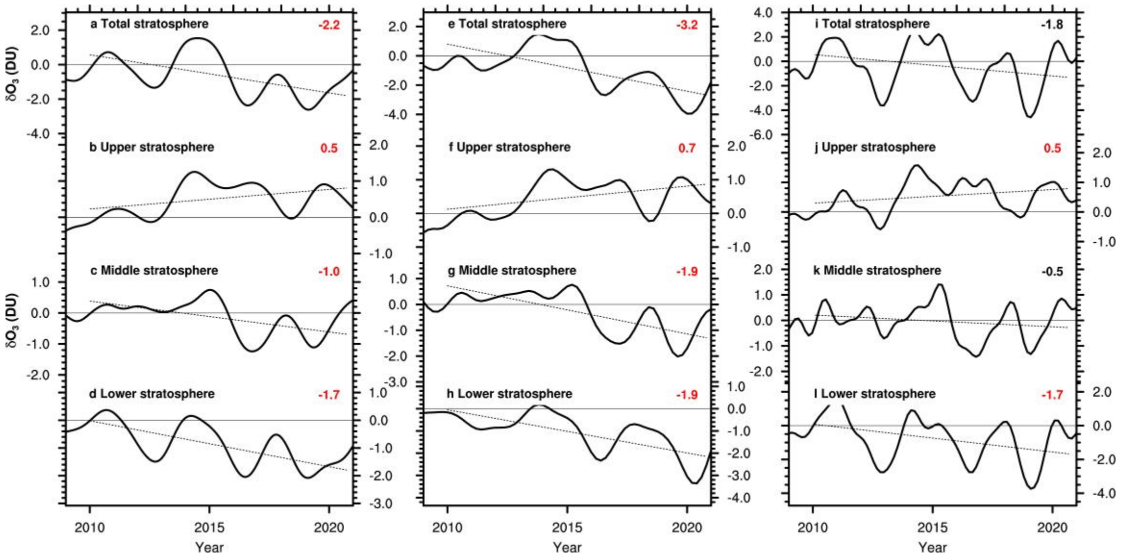

Fig. 4. Partial column ozone trends between different pressure levels from 2010 to 2020 in the 30°S–60°N latitudinal belt. Partial column ozone changes between 100 and 1 hPa (a, e, i), between 10 and 1 hPa (b, f, j), between 32 and 10 hPa (c, g, k), and between 100 and 32 hPa (d, h, l). The ozone data are from SWOOSH. For data information, please refer to the Methods section. Panels (a–d) are for 12 months, (e–h) are for May–September, and (i–l) are for October–April. The linear trends (black straight dotted lines) were calculated by linear regression. The number close to right-hand *y*-axis is the linear trend value (unit: DU/decade) of TCO changes from 2010 to 2020. Red and black values are significant and non-significant, respectively, at the 2σ level using the Student's *t*-test. Low-pass filtering (to filter out periods of less than 3 years) was performed on the TCO changes before calculating the trend.

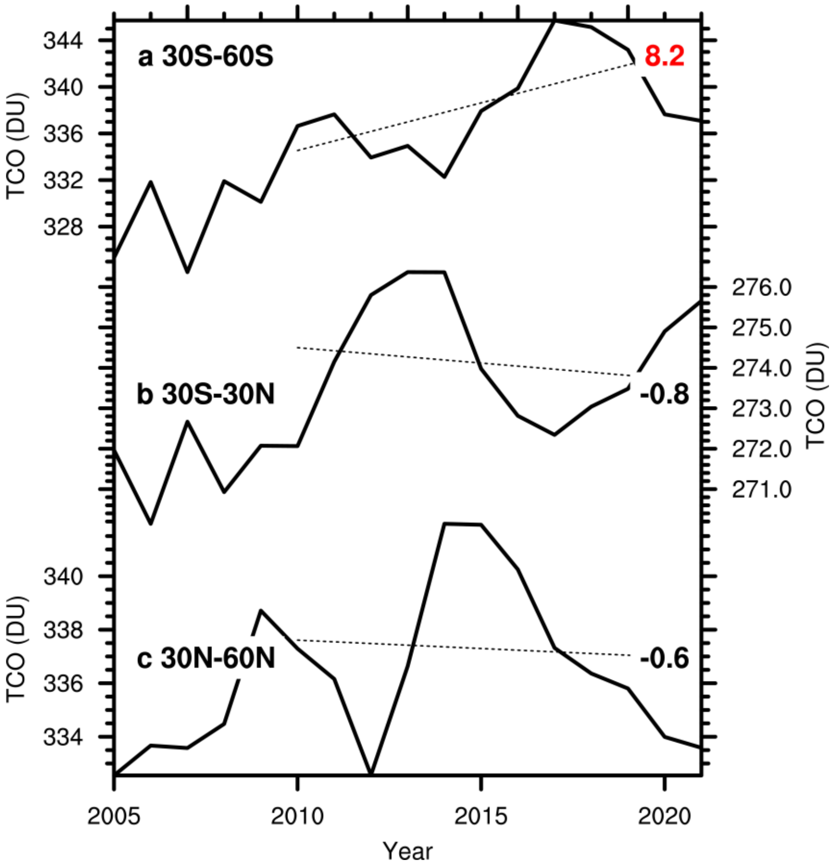

Fig. 5. TCO changes between different latitudinal belts from 2005 to 2020 for the May–September average based on the experiment of the TOMCAT/SLIMCAT model. TCO changes between 60°S and 30°S (a), between 30°S and 30°N (b), and between 30°N and 60°N (c). Linear trends (black straight dotted lines) are calculated by linear regression. The number close to the right-hand *y*-axis is the linear trend value (unit: DU/decade) for the period 2010–2020. Red and black values are significant and non-significant, respectively, at the 2σ level using the Student's *t*-test. A three-point running average was performed on the TCO changes before calculating the trend.

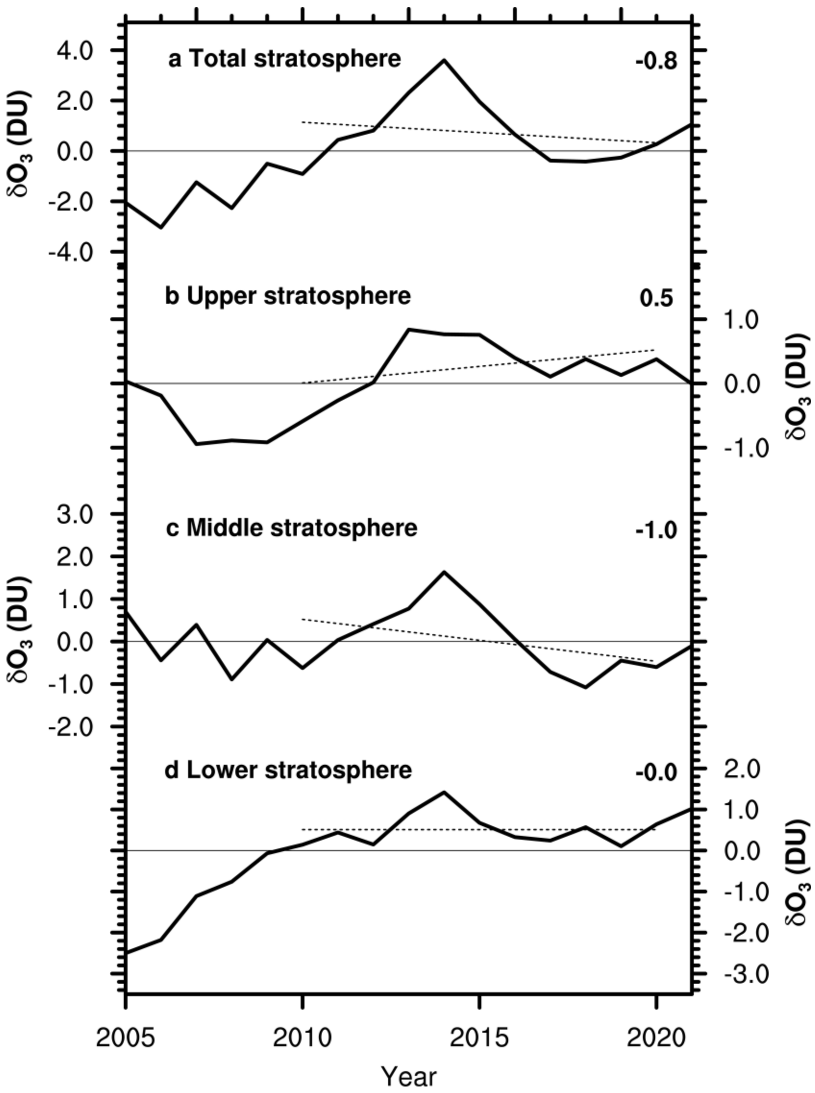

Fig. 6. Partial column ozone changes between different pressure levels in the 30°S–60°N latitudinal belt from 2005 to 2020 for the May–September average based on the experiment of the TOMCAT/SLIMCAT model. Partial column ozone changes between 100 and 1 hPa (a), between 10 and 1 hPa (b), between 32 and 10 hPa (c), and between 100 and 32 hPa (d). The linear trends (black straight dotted lines) were calculated by linear regression. The number close to the right-hand *y*-axis is the linear trend value (unit: DU/decade) for the period 2010–2020. Red and black values are significant and non-significant, respectively, at the 2σ level using the Student's *t*-test. A three-point running average was performed on the TCO changes before calculating the trend.

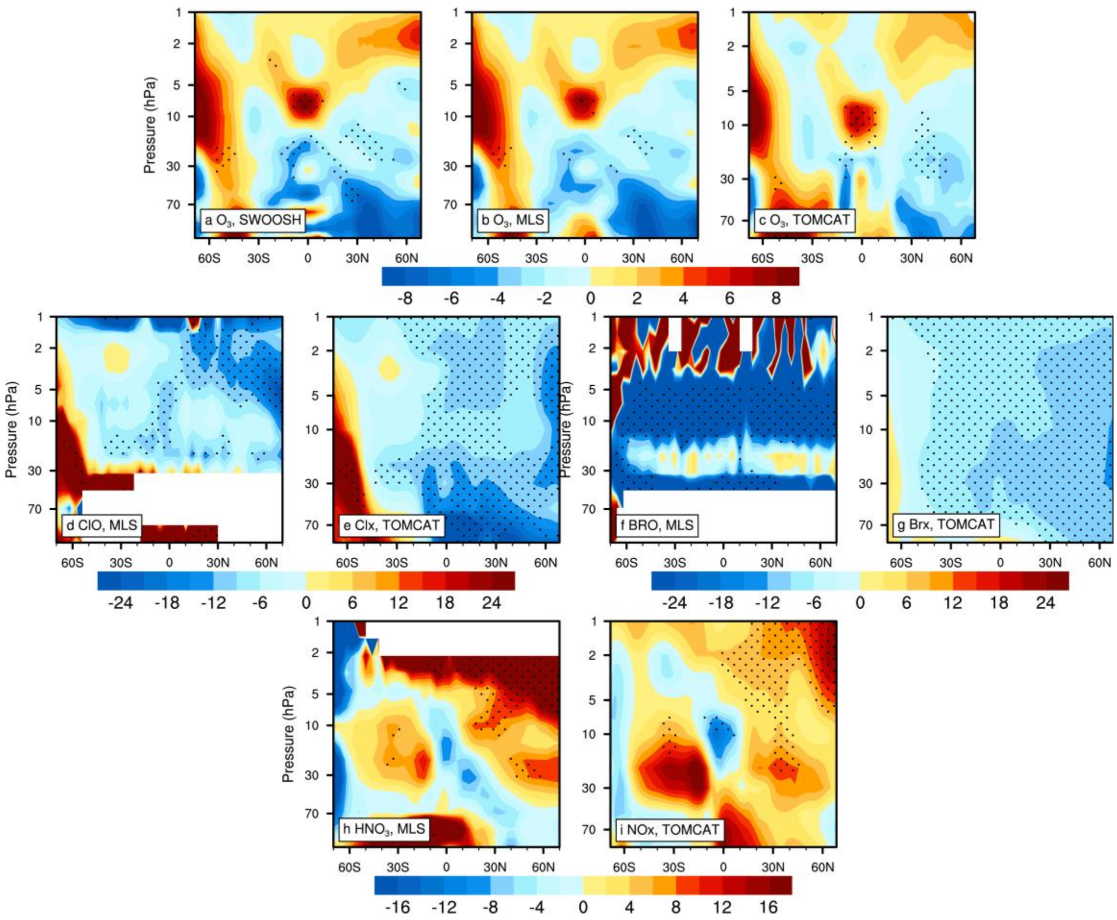

Fig. 7. Fractional trend distributions of zonally averaged chemical components for May–September from 2010 to 2020 with respect to the multi-year average. (a–c) O_3; (d) ClO; (e) CL+ClO; (f) BrO; (g) BR+BrO; (h) HNO_3; (i) NO+NO_2. Panel (a) is from SWOOSH; panels (b, d, f, h) are from the MLS dataset; and panels (c, e, g, i) are from the TOMCAT/SLIMCAT simulation. The fractional trend was calculated by the linear trend divided by the average (unit: %/decade). Linear trends were calculated by linear regression. Low-pass filtering (to filter out periods of less than 3 years) was performed on the chemical component changes before calculating the trend. The dotted area indicates statistical significance at the 2σ level based on the Student's *t*-test.

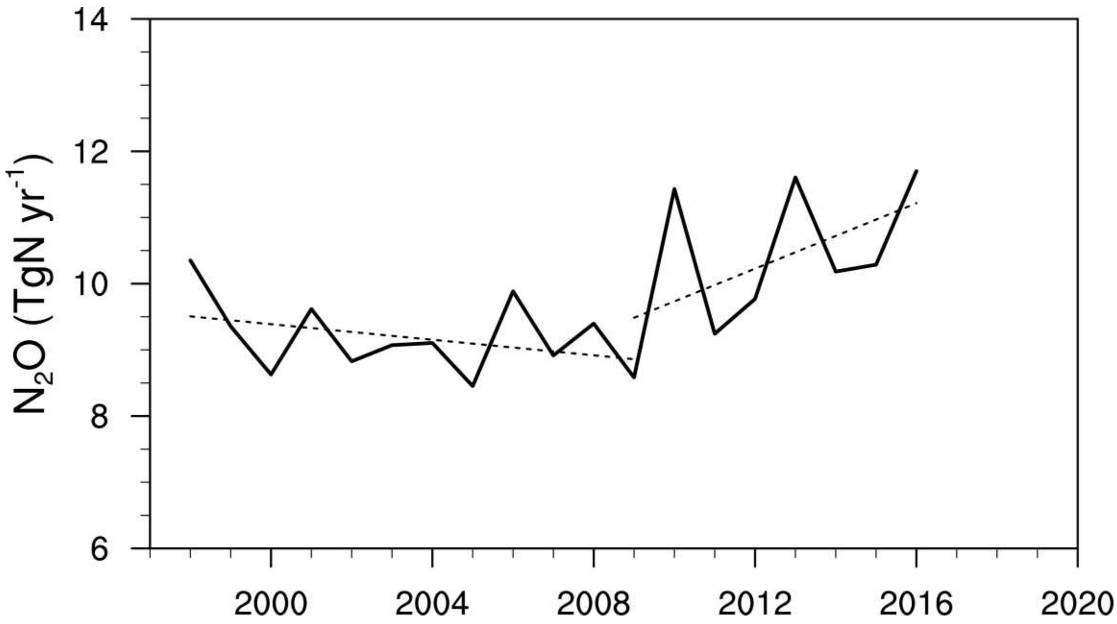

Fig. 8. Annual averaged global surface N_2O emissions. Linear trends (black straight dotted lines) are calculated by linear regression; two periods: 1998–2009 and 2009–2016. For details of the surface N_2O emissions data, please refer to Thompson et al. (2019).

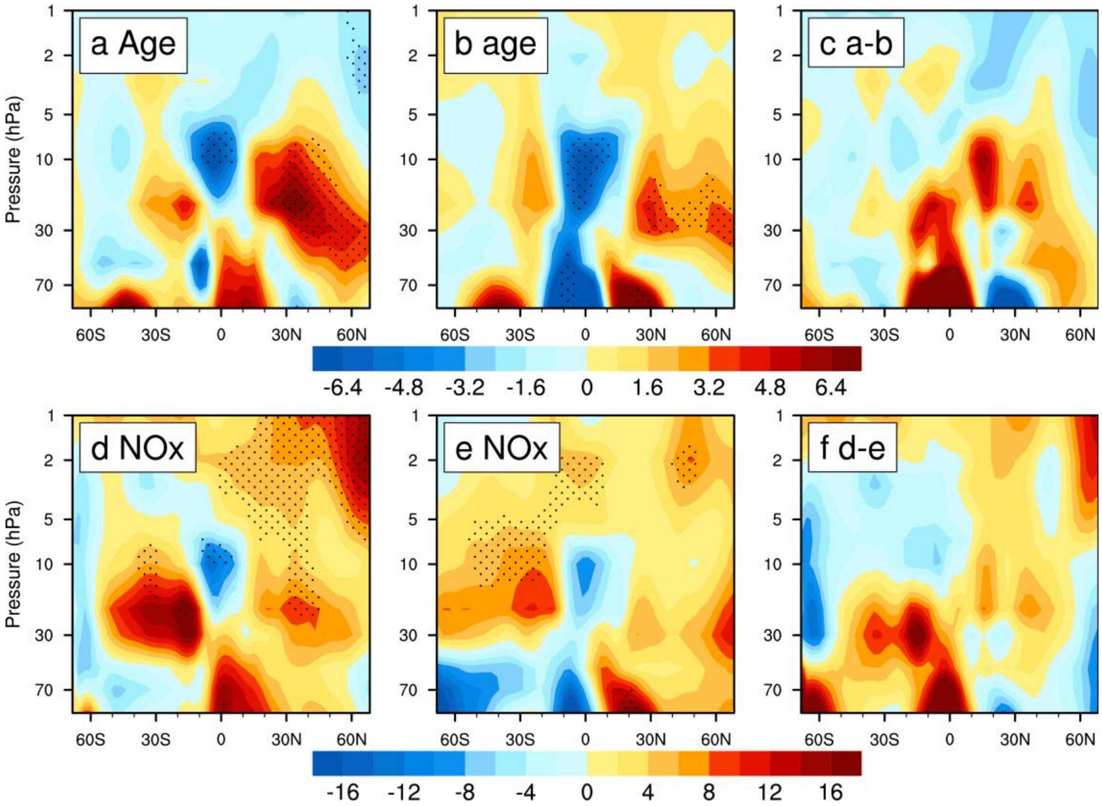

Fig. 9. Fractional trend distributions of the zonally averaged age-of-air and NO_x from 2010 to 2020 based on the experiment of the TOMCAT/SLIMCAT model. Age-of-air (a, b) and $NO+NO_2$ (d, e) for May–September (a, d) and October–April (b, e). The fractional trend was calculated by the linear trend divided by the average (unit: %/decade). Linear trends were calculated by linear regression. Low-pass filtering (to filter out periods of less than 3 years) was performed on the chemical component changes before calculating the trend. The dotted area indicates statistical significance at the 2σ level based on the Student's *t*-test. (c) = (a) − (b), (f) = (d) − (e).